

Physics with a very long neutrino factory baseline

RAJ GANDHI^a, WALTER WINTER^b

^a*Harish-Chandra Research Institute,
Jhusi, Allahabad–211 019, India*

^b*Institut für Theoretische Physik und Astrophysik, Universität Würzburg
D-97074 Würzburg, Germany*

June 28, 2021

Abstract

We discuss the neutrino oscillation physics of a very long neutrino factory baseline over a broad range of lengths (between 6 000 km and 9 000 km), centered on the “magic baseline” ($\sim 7\,500$ km) where correlations with the leptonic CP phase are suppressed by matter effects. Since the magic baseline depends only on the density, we study the impact of matter density profile effects and density uncertainties over this range, and the impact of detector locations off the optimal baseline. We find that the optimal constant density describing the physics over this entire baseline range is about 5% higher than the average matter density. This implies that the magic baseline is significantly shorter than previously inferred. However, while a single detector optimization requires fine-tuning of the (very long) baseline length, its combination with a near detector at a shorter baseline is much less sensitive to the far detector location and to uncertainties in the matter density. In addition, we point out different applications of this baseline which go beyond its excellent correlation and degeneracy resolution potential. We demonstrate that such a long baseline assists in the improvement of the θ_{13} precision and in the resolution of the octant degeneracy. Moreover, we show that the neutrino data from such a baseline could be used to extract the matter density along the profile up to 0.24% at 1σ for large $\sin^2 2\theta_{13}$, providing a useful discriminator between different geophysical models.

^aEmail: raj@mri.ernet.in

^bEmail: winter@physik.uni-wuerzburg.de

1 Introduction

Input from experiments is central to the search for a theory beyond the Standard Model of elementary particle physics. Given the extraordinary robustness of this model, such input necessarily requires precision measurements of the relevant parameters in order to reveal discrepancies, which, in turn, would provide clues to a higher theory. It is evident that at the present time, in addition to the upcoming Large Hadron Collider [1], neutrino physics provides an unprecedented opportunity to move successfully towards this goal via increasingly accurate measurements of neutrino mass squared differences and mixing parameters. These parameters have only been partially revealed by experiments so far (see, *e.g.*, Refs. [2–5]). A large number of experiments are thus planned or currently under way to achieve this goal. Among these, in the near future, are neutrino beam experiments [6–8] and reactor experiments [9–12]. What may be learnt from these experiments depends, however, on how large the mixing angle θ_{13} is. In particular, some of the important issues crucial to the formulation of a unified theory, such as the value of the CP violating parameter δ_{CP} , or the nature of the neutrino mass hierarchy, may not be determined by these experiments. With present bounds ($\sin^2 \theta_{13} = 0_{-0}^{+0.047}$, $\delta_{\text{CP}} = 0_{-\pi}^{+\pi}$ [5]), already restricting θ_{13} fairly stringently, it could, in principle, be very small. This would inevitably result in the determination of important physics being relegated to an advanced future facility, such as a neutrino factory [13–15].

The unprecedented reach and accuracy of a neutrino factory, and the broad scope of physics that can be explored has been discussed in detail in several studies (see, *e.g.*, Refs. [16–23]). Much of the science centers around isolating the matter effects in neutrino oscillations and determining how the various degeneracies and correlations in the measured quantities can be successfully resolved to obtain unambiguous physics. The presence of intertwined parameters and effects thus requires careful phenomenological and optimization studies in order to best determine the specifications of the source facility and the location of detectors. One of the significant results of these efforts is the identification of the “magic baseline” for neutrino passage through the Earth, which is a baseline between about 7 000 and 7 500 km [24, 25]. Clean measurements of $\sin^2 2\theta_{13}$ and the mass hierarchy are possible due to the disappearance of CP effects at this baseline. Most recently, these issues have been studied in detail from the point of view of the optimization with respect to $\sin^2 2\theta_{13}$, the mass hierarchy, and CP violation sensitivities, as well as the measurement of the leading atmospheric parameters in Ref. [23]. The conclusion from this study is that an optimal advanced neutrino factory would be operated with two detector locations, one in the range between 3 000 km to 5 000 km, and the second at or around the magic baseline. We recall that the magic baseline depends only on the matter density, arising from the condition $\sqrt{2}G_F n_e L = 2\pi$, where G_F is the weak coupling constant and n_e is the electron number density. Obviously, the exact density profile plays an important role for the physics potential of the very long baseline, whereas the oscillation parameter values and neutrino energies are (almost) irrelevant. In comparison, the optimal “short” baseline length depends on the oscillation parameters, but the baseline window is large enough such that one does not have to worry too much about the actual parameters and the matter density profile for the choice of the detector location. Since the precise location of a detector is a function of many variables, a good fraction of

which may be unrelated to physics, it is necessary to study the impact of locating the second detector not at the optimal magic length, but somewhere in the range between 6 000 km and 9 000 km. In addition to this geographical uncertainty, the effects of the matter density profile and its uncertainties on the optimization are significant. In this study, we explore these questions by introducing a realistic matter density profile model in Sec. 4, and by examining the physics consequences of this model in Sec. 5. Note that in our scenario, the neutrino factory feeds two detectors, one at $L_1 = 4\,000$ km [23], the other at L_2 between 6 000 km and 9 000 km. We study, as new applications, the θ_{13} precision measurement in Sec. 6 and the octant degeneracy resolution in Sec. 7, and we sketch the physics case for such a baseline in Sec. 9. We believe that the investigation of these questions is especially germane in the light of the presently ongoing International Scoping Study for a future neutrino factory and superbeam facility [26]. As an interesting application for geophysics, we also demonstrate how neutrino measurements may help to extract information about the matter density profile and to discriminate between different Earth density models in Sec. 8.

2 Physics at the Magic Baseline

It was noticed in Ref. [24, 25] that the condition $\sqrt{2}G_F n_e L = 2\pi$ leads to a disappearance of CP violation effects and related degeneracies in $P_{e\mu}$. Several studies have subsequently explored the physics possibilities resulting from the enhanced matter effects at and around this baseline, see, *e.g.*, Refs. [23, 27–32]. A recent closer examination of the phenomenology has been done in Ref. [33]. In this section we review the salient features and reasons which make this baseline a phenomenologically attractive one. We start with an approximate analytical expression for $P_{e\mu}$, which is accurate up to second order in the combination of two parameters which can (usually) be treated as small, namely $\alpha \equiv \frac{\Delta m_{21}^2}{\Delta m_{31}^2} \sim \pm 0.03$ and $\sin 2\theta_{13}$ [19, 29, 34]:

$$\begin{aligned}
P_{e\mu} &\simeq \sin^2 2\theta_{13} \sin^2 \theta_{23} \frac{\sin^2[(1 - \hat{A})\Delta]}{(1 - \hat{A})^2} \\
&\pm \alpha \sin 2\theta_{13} \sin 2\theta_{12} \sin 2\theta_{23} \sin \delta_{\text{CP}} \sin(\Delta) \frac{\sin(\hat{A}\Delta)}{\hat{A}} \frac{\sin[(1 - \hat{A})\Delta]}{(1 - \hat{A})} \\
&+ \alpha \sin 2\theta_{13} \sin 2\theta_{12} \sin 2\theta_{23} \cos \delta_{\text{CP}} \cos(\Delta) \frac{\sin(\hat{A}\Delta)}{\hat{A}} \frac{\sin[(1 - \hat{A})\Delta]}{(1 - \hat{A})} \\
&+ \alpha^2 \cos^2 \theta_{23} \sin^2 2\theta_{12} \frac{\sin^2(\hat{A}\Delta)}{\hat{A}^2}. \tag{1}
\end{aligned}$$

In the above, $\Delta \equiv \frac{\Delta m_{31}^2 L}{4E_\nu}$ and $\hat{A} \equiv \frac{2\sqrt{2}G_F n_e E}{\Delta m_{31}^2}$ and the θ_{ij} are the usual neutrino mixings. The defining condition for the magic baseline is

$$\sin(\hat{A}\Delta) = 0 \quad \Rightarrow \quad \frac{G_F n_e L}{\sqrt{2}} = \pi \tag{2}$$

for the first (shortest baseline) non-trivial solution. It is apparent that in this case only the first term in Eq. (1) remains, which means that any dependence on δ_{CP} is removed. It

is important to note that Eq. (2) is also the defining equation for the refraction length of a medium [35]. For large matter densities and high energies beyond the resonance energy of the medium, the effective neutrino oscillation length in matter approaches the refraction length. Moreover, at these baselines and energies, the oscillation length in matter is driven by Δm_{21}^2 , and not Δm_{31}^2 . When the matter oscillation length equals the refraction length, the phase in matter for oscillations driven by the solar mass difference becomes 2π , and terms containing Δm_{21}^2 and δ_{CP} in the above expansion drop out of the probability [33].

We stress that these statements related to the magic baseline are subject to corrections from the following: a) The accuracy and the validity of the above expansion in α and $\sin 2\theta_{13}$, b) the validity of the constant density approximation, c) our knowledge of the Earth's density profile, and d) the correctness of choosing the average density as the constant density which determines the magic baseline via Eq. (2) above.

The accuracy and validity of various analytical series expansions for matter probabilities has been discussed in Ref. [29]. In general, one can choose to expand either in α alone, or in $\sin 2\theta_{13}$ alone, retaining terms up to first order in one of these parameters while treating the other parameter exactly. Alternatively, one can choose to treat both as small parameters (*i.e.*, do a double expansion), and keep terms up to second order, as we have done above in Eq. (1). The single expansion in α retains the exact dependence in $\sin 2\theta_{13}$, and hence is more accurate than the double expansion for values of $\sin 2\theta_{13}$ close to the upper bound. It is valid for $\alpha \Delta \equiv \frac{\Delta m_{21}^2 L}{4E\nu} \ll 1$ (which translates to $L/E \ll 10^4$ km/GeV), *i.e.*, when the vacuum oscillation length defined by the “solar” mass squared difference is much larger than L . On the other hand, the single expansion in $\sin 2\theta_{13}$ is most accurate when this parameter assumes values which are very small ($\sim 10^{-3}$ or less). The double expansion in Eq. (1) is, in general, robust over a wide range of parameters (in particular, $\sin 2\theta_{13}$, L , and E) in the sense that relative errors in $P_{\mu e}$, $P_{\mu\tau}$, and $P_{\mu\mu}$ are restricted to be below 5%. In terms of validity, errors resulting from its use are lowest (below 1%) when $\alpha \Delta \equiv \frac{\Delta m_{21}^2 L}{4E\nu} \ll 1$, *i.e.*, $L/E \ll 10^4$ km/GeV, and when $\sin 2\theta_{13}$ is small but still above the range which makes the single expansion in it preferable. As far as the defining equation for the magic baseline Eq. (2) is concerned, note that it is directly obtained from the double expansion. Therefore, these constraints on the validity of the expansion need to be kept in mind when drawing conclusions about results from a detector located at $L = L_{\text{Magic}}$, especially when precision of a few percent is important.¹

As a first approximation, Eq. (2) can be usefully rewritten as

$$L_{\text{Magic}} \simeq \frac{\sqrt{2}\pi}{G_F n_e} \simeq 7800 \frac{4.2 \text{ g/cm}^3}{\bar{\rho}(L)} \text{ km} \quad (3)$$

where

$$\bar{\rho}(L) = \frac{1}{L} \int_0^L \rho(x) dx \quad (4)$$

¹An approach independent of an analytical expansion would numerically search for the minimal dependence on the solar amplitude contributions to the transition probability, but it would still be subject to uncertainties in our knowledge of the density profile.

is the baseline-averaged density. Solving this equation, we find $L_{\text{Magic}} \simeq 7630$ km and $\bar{\rho}(7630 \text{ km}) \simeq 4.29 \text{ g cm}^{-3}$. Most studies in the literature have used $\bar{\rho}(L)$ in calculations, and have drawn conclusions based on it as the preferred choice for the constant density. There is no doubt that the simplified analysis based on the constant density approximation has provided many insights into the effect of matter oscillations on neutrinos as they travel through the Earth. However, as precision assumes increasing importance in the determination of neutrino parameters, it is important to ask how well $\bar{\rho}(L)$ reproduces the profile effect for a given baseline. In particular, we will discuss if $\bar{\rho}(L)$ is indeed the best choice for the constant density to reproduce physics. We will introduce a constant reference density for that purpose which can be different from $\bar{\rho}(L)$, and examine its dependence on the baseline, on the neutrino oscillation parameters (such as $\sin^2 2\theta_{13}$ and δ_{CP}), and on the oscillation channel that one is observing. In the next section, we describe the simulation methods employed by us, prior to addressing this question in detail in Sec. 4, where we also describe our procedure for modeling the Earth’s density profile.

Finally, we stress two important features of the magic baseline relevant to measurements of the Earth’s matter density. First, the clean dependence of physics at the magic baseline on the matter density due to the independence of CP and solar mass-squared difference terms suggests that it could be an optimal baseline for Earth density measurements. In other words, if the density was considered as just another parameter to be determined via neutrino experiments, this determination would be cleanest and most uncluttered by correlations if it was done at the magic baseline. Secondly, we note that the condition $\sin(\hat{A}\Delta) = 0$ automatically tells us that the sensitivity to any change in the assumed constant density (*i.e.*, the derivative) is maximal here for the terms proportional to $\sin(\hat{A}\Delta)$, and consequently, is expected to be high for the full probability. This fact can be usefully employed to extract information about the density. These ideas are explored further in Sec. 8 of this work.

3 Simulation methods

Our simulation is based upon the standard neutrino factory in Refs. [22, 23] with a muon energy $E_\mu = 50$ GeV and a 50 kt magnetized iron detector. We use a total luminosity of 4.24×10^{21} useful muon decays and 4.24×10^{21} useful anti-muon decays, which can be achieved by four years of operation in each polarity at 1.06×10^{21} useful parent decays/year, or by eight years of simultaneous operation of both polarities at 0.53×10^{21} useful parent decays/year/polarity. The neutrino factory uses both the muon neutrino/anti-neutrino appearance ($\nu_e \rightarrow \nu_\mu$) and disappearance ($\nu_\mu \rightarrow \nu_\mu$) channels. As in Ref. [23], we use a data sample without charge identification for the disappearance channels to avoid cuts from the charge identification, and therefore increase statistics. For a more detailed description, see Refs. [22, 23].

In order to perform the simulation, we use the GLoBES software [36]. Since it is relevant for this study, let us focus on the way GLoBES treats the matter density. In GLoBES, the

²Note the non-trivial inter-dependence inherent in seeking a solution to Eq. (3), since $\bar{\rho}(L)$ in the equation depends actually on L_{Magic} .

matter density of each experiment is implemented as yet another oscillation parameter, *i.e.*, the total systematics χ^2 for one experiment is a function of the oscillation parameters and the matter density. For two experiments, the systematics χ_{sys}^2 is then computed as

$$\begin{aligned} \chi_{\text{sys}}^2(\theta_{12}, \theta_{13}, \theta_{23}, \delta_{\text{CP}}, \Delta m_{21}^2, \Delta m_{31}^2, \hat{\rho}_1, \hat{\rho}_2) &= \chi_{L_1}^2(\theta_{12}, \theta_{13}, \theta_{23}, \delta_{\text{CP}}, \Delta m_{21}^2, \Delta m_{31}^2, \hat{\rho}_1) + \\ &+ \chi_{L_2}^2(\theta_{12}, \theta_{13}, \theta_{23}, \delta_{\text{CP}}, \Delta m_{21}^2, \Delta m_{31}^2, \hat{\rho}_2) \end{aligned} \quad (5)$$

for two different baselines L_1 and L_2 with different density scaling factors $\hat{\rho}_1$ and $\hat{\rho}_2$, where the oscillation probabilities in $\chi_{L_1}^2$ and $\chi_{L_2}^2$ depend on the respective density scaling factors. GLOBES allows arbitrary density profiles, which are scaled by these density scaling factors $\hat{\rho}$. For instance, for a constant density profile with density ρ_0 , the actual density will be computed as $\hat{\rho} \cdot \rho_0$. For an arbitrary profile, $\hat{\rho}$ acts as an overall normalization factor with which the density in each layer is multiplied. As the next step in the χ^2 calculation, the external input is added as

$$\tilde{\chi}^2 = \chi_{\text{sys}}^2(\theta_{12}, \theta_{13}, \theta_{23}, \delta_{\text{CP}}, \Delta m_{21}^2, \Delta m_{31}^2, \hat{\rho}_1, \hat{\rho}_2) + \left(\frac{\hat{\rho}_1 - 1.0}{\sigma_{\hat{\rho}_1}} \right)^2 + \left(\frac{\hat{\rho}_2 - 1.0}{\sigma_{\hat{\rho}_2}} \right)^2 + \dots, \quad (6)$$

where the dots correspond to other potential external constraints (such as for the solar parameters). Typically, we use $\sigma_{\hat{\rho}} = 0.05$, corresponding to a 5% overall normalization uncertainty of the density profile. This $\tilde{\chi}^2$ is then marginalized over the unwanted oscillation parameters and density scaling factors. The marginalization procedure corresponds to the projection of the eight-dimensional fit manifold onto the targeted sub-space. For example, for a $\sin^2 2\theta_{13}$ precision measurement, all other parameters and density scaling factors are marginalized over. For a $\hat{\rho}_2$ precision measurement (corresponding to the relative error for a constant density), all oscillation parameters *and* $\hat{\rho}_1$ are marginalized over, as well as $\sigma_{\hat{\rho}_2} \rightarrow \infty$.³ Therefore, there is no *a priori* difference between the oscillation parameters and density scaling factors.

In some cases, we will even use a more detailed approach with different parts of the density profile being treated with different scaling factors. In this case, one has to perform the density marginalizations in GLOBES manually, *i.e.*, set the density profile in each step and manually scan the density scaling factors of the different sub-profiles. For example, we will use this approach to measure the lower mantle density only, while we impose an uncertainty on the upper mantle density of the Earth.

For the oscillation parameters, we use $\sin^2 2\theta_{12} = 0.83$, $\sin^2 2\theta_{23} = 1$, $\Delta m_{21}^2 = 8.2 \cdot 10^{-5} \text{ eV}^2$, $\Delta m_{31}^2 = 2.5 \cdot 10^{-3} \text{ eV}^2$, and a normal hierarchy unless stated otherwise (see, *e.g.*, Refs. [2, 5, 37–39]). In addition, we assume a 5% external measurement for Δm_{21}^2 and θ_{12} from solar experiments (see, *e.g.*, Ref. [38]). We furthermore include matter density uncertainties of the order of 5% [40, 41] uncorrelated between the different baselines – unless we measure the matter density. In principle, we include all parameter correlations and discrete degeneracies [20, 24, 42, 43] where applicable. However, the octant degeneracy will not be present for maximal mixing.

³Note that in this case, we still impose an uncertainty on $\hat{\rho}_1$, because $\hat{\rho}_1$ is, in the most conservative case, fully uncorrelated with $\hat{\rho}_2$.

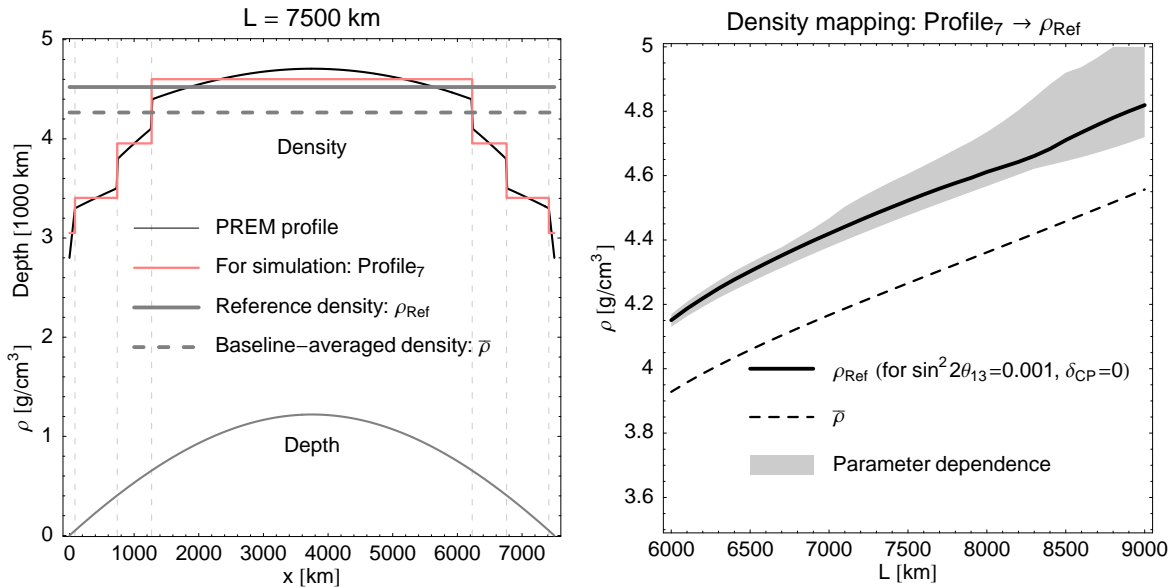


Figure 1: Mapping from PREM profile via the simulation profile “Profile₇” to our constant reference density ρ_{Ref} . The left plot shows several possible matter density profiles as function of the propagation length x for a fixed baseline $L = 7500$ km, as well as the depth as function of baseline. The right plot shows our constant reference density ρ_{Ref} corresponding to Profile₇ in the left plot as function of the baseline L (solid curve) – see text for explanation of the mapping. The baseline-averaged density $\bar{\rho}$ is shown for comparison as well, and the parameter dependence of the mapping on $\sin^2 2\theta_{13}$ and δ_{CP} is illustrated by the gray-shaded area.

4 Modeling the density profile and determining the optimal constant density

Most simulations in the literature so far have used the baseline-averaged matter density calculated using Eq. (4), where $\rho(x)$ is calculated along the baseline using the PREM profile. Since the magic baseline is mainly determined by the matter density, this description may not be accurate enough to find the optimal detector location (see, *e.g.*, Ref. [44] for a discussion at the probability level). Therefore, we follow a different approach in this section, and seek a constant density that best simulates the PREM profile. We label this density as the “reference density”, ρ_{Ref} .

To begin with, we note that a numerical simulation cannot use the unmodified PREM profile because most numerical techniques are based on the re-diagonalization of the Hamiltonian in constant matter density (*cf.*, for instance, Ref. [45]). Therefore, the PREM profile has to be made accessible to numerical simulations, *i.e.*, it has to be accurately modeled. One possibility is to use a Fourier expansion [46], which, however, does not describe the edges very accurately and is not easily implementable in GLOBES. Therefore, we use a different approach, which is suitable for the baseline window of interest here (6000 km to 9000 km). We illustrate this model, which we call “Profile₇” (because of seven layers) in Fig. 1 and show

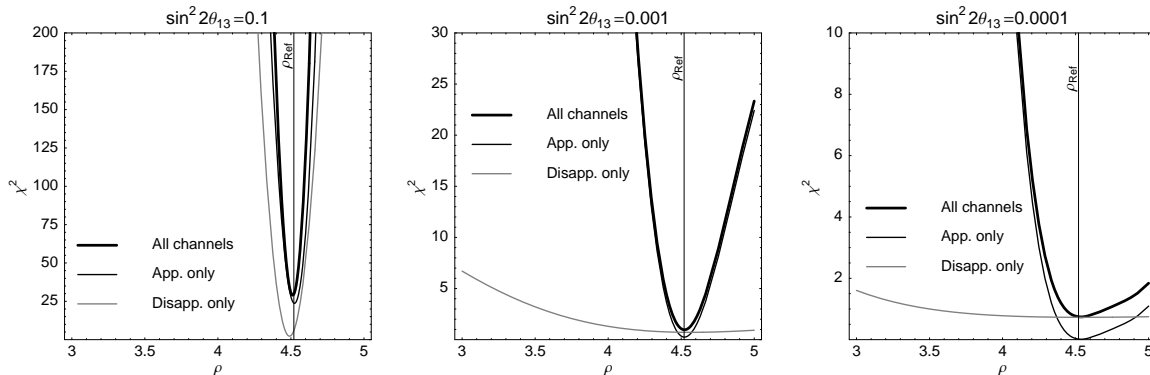


Figure 2: χ^2 between a simulated Profile₇ and a fit constant density profile as a function of the fit density ρ . The different panels correspond to three different values of $\sin^2 2\theta_{13}$ (see plot labels). In each plot, we show three different oscillation channel choices (appearance only, disappearance only and all channels combined). The reference density sits at the minimum of the χ^2 for all channels combined (chosen for $\sin^2 2\theta_{13} = 0.001$), and is marked by the vertical lines in all panels. Note that the scales for the vertical axes differ from each other in the three panels. In this figure, $\delta_{\text{CP}} = 0$ and $L = 7500$ km.

how it compares to the PREM profile. For any baseline between 6 000 km and 9 000 km, the profile looks very similar to the one for $L = 7500$ km shown in the left panel of Fig. 1. We compute Profile₇ for any given L in this range by choosing the density jumps as edges between two layers (such as between upper mantle and lower mantle of the Earth). Each layer is then simulated by using the average density given by Eq. (4) within that layer. Note that although the use of more steps would make the modeling more accurate, any realistic simulation seeks to use an optimal number that retains accuracy while keeping the computational time within reasonable limits. We have checked that Profile₇ reproduces the results of a simulation with significantly more steps with sufficient accuracy.

As mentioned above, we seek an optimal constant density which can be reliably used as a reference density in lieu of full numerical simulations. We define this to be the constant density which simulates the PREM profile best and denote it as ρ_{Ref} . In order to relate ρ_{Ref} to Profile₇ for any given baseline, we use the χ^2 from the complete neutrino factory simulation described in the last section (including neutrino and antineutrino appearance and disappearance). We identify the ρ_{Ref} which simulates Profile₇ best by requiring that χ^2 be minimal between a constant fit profile with ρ_{Ref} and the simulated Profile₇, for a given set of fixed oscillation parameters. This means that we minimize the contribution from the leading (zeroth) order profile effect to the total χ^2 . We illustrate this process in Fig. 2, in which we show the variation of χ^2 with the choice of the constant density ρ for different values of $\sin^2 2\theta_{13}$ and for different oscillation channel choices. The reference density is marked by the vertical lines as the minimum of the χ^2 between the constant density profile and Profile₇ (obtained for $\sin^2 2\theta_{13} = 0.001$, $\delta_{\text{CP}} = 0$). In all three panels (each representing a different value of $\sin^2 2\theta_{13}$), the appearance channel dominates the determination of ρ_{Ref} , but for large $\sin^2 2\theta_{13}$, the disappearance channel also contributes significantly. For small $\sin^2 2\theta_{13}$, the appearance channel χ^2 becomes much more sensitive to deviations from ρ_{Ref} than the

disappearance channel. The reason is that the disappearance channel is almost in the two-flavor vacuum regime described by $\nu_\mu \leftrightarrow \nu_\tau$ oscillations for $\sin^2 2\theta_{13} \rightarrow 0$, *i.e.*, independent of matter effects. Therefore, inaccuracies in the estimation of the constant reference density are much less important for the disappearance channel than for the appearance channel.

We show our choice for $\rho_{\text{Ref}}(L)$ as function of baseline as the solid curve in Fig. 1 (right), which was obtained for the reference values $\sin^2 2\theta_{13} = 0.001$ and $\delta_{\text{CP}} = 0$. Expectedly, this mapping depends on the choice of oscillation parameters, as illustrated in Fig. 1 (right panel) by the shaded area obtained for different sets of parameters. We find that the δ_{CP} -dependence for large values of $\sin^2 2\theta_{13}$ is very mild, reflecting the dominance of matter effects. As shown above, the minimum χ^2 between the profiles ρ_{Ref} and Profile₇ is rather large ($\chi^2 \sim 15$ to 35) and the function $\chi^2(\rho)$ is rather steep for the large $\sin^2 2\theta_{13}$ case. On the other hand, for small values of $\sin^2 2\theta_{13}$, the dependence on δ_{CP} is stronger, but the minimum χ^2 between the profiles ρ_{Ref} and Profile₇ is rather small ($\chi^2 \sim 1$ to 10), while the function $\chi^2(\rho)$ is more shallow. Therefore, we conclude that the parameter dependence in Fig. 1, right (shaded area) may actually not be very significant, either because there is no significant δ_{CP} -dependence (large $\sin^2 2\theta_{13}$), or because the statistical contribution from deviations is small (small $\sin^2 2\theta_{13}$). We will test this hypothesis later in full numerical simulations using different profiles. Note that we will simulate any baseline shorter than 6 000 km as usual with $\bar{\rho}$.

A noteworthy point from Fig. 1 is that ρ_{Ref} is consistently higher than $\bar{\rho}(L)$ by about 5%. This reflects the dominance of high density regions in the lower mantle (*cf.*, left panel of Fig. 1). The fact that matter effects at short baselines are relatively suppressed (irrespective of the density profile) has been discussed in Ref. [47]. Thus, in our case, the high density central region of the profile contributes with a higher weight compared to the low density regions. At short baselines, transition amplitudes for neutrinos can be treated perturbatively, and the leading order terms reflect the contributions of the matter independent off-diagonal terms of the effective Hamiltonian, whereas matter contributions reside in the diagonal terms. None of this information finds its way into the simple averaging that determines $\bar{\rho}(L)$. Clearly, an optimized constant density for each channel offers superior accuracy compared to simple averaging since it incorporates the effects of matter on transition amplitudes in a weighted way. This has significant consequences for determining the length of the magic baseline. For instance, we see from Fig. 1 that the ρ_{Ref} corresponding to 7 600 km is 4.5 g/cm^3 rather than 4.2 g/cm^3 . Therefore, the magic baseline length becomes an estimated $\sim 7 300$ km according to Eq. (3), *i.e.*, several hundred kilometers shorter. It is thus important that prior to fixing the location of the far detector, an optimized reference density be used as opposed to using $\bar{\rho}(L)$. This sensitivity to the density changes if two detectors are used, one at $L_1 = 4 000$ km, and the other in the range between 6 000 km and 9 000 km. We study this combination in the next section.

5 How precisely does one have to tune very long baseline length?

In Ref. [23], the combination of a short baseline $L \simeq 4 000$ km optimal for CP violation and the “magic baseline” $L \simeq 7 500$ km optimal for degeneracy resolution and mass hierarchy

determination was found to have an excellent physics potential. The choice of this specific $L = 7\,500$ km was (in this and earlier studies [25]) based on the $\sin^2 2\theta_{13}$ sensitivity being optimal there due to vanishing δ_{CP} effects. While it was found that the short baseline is rather insensitive to the specific baseline length in a window between about 3 000 and 5 000 km, the magic baseline optimum was found in a very small window of L which only depends on the matter density profile. In this section, we therefore discuss how precisely one has to place the detector on the magic baseline, a question very relevant for the selection of detector locations, and the extent of the impact from profile effects and inaccurately estimated profiles.

Before we actually discuss the impact of the long baseline choice on the physics potential, let us focus on the most important questions:

1. *Detector location:* How much sensitivity does one lose if one moves the detector slightly off the optimal length?
2. *Unknown matter density:* The length of the magic baseline depends on the matter density. What happens if the matter density along the baseline has been misjudged within current geophysical uncertainties?
3. *Profile effects:* How well does a constant density simulate the matter density profile? Does that affect the baseline optimization? Is the actual sensitivity better or worse compared to using a constant density?

In order to answer question 1, we will show the sensitivities in a window between 6 000 and 9 000 km in very small steps. For the complete picture, see, *e.g.*, Ref. [23]. For question 2, we will show the results for ρ_{Ref} as well as the most conservative estimates $0.95 \rho_{\text{Ref}}$ and $1.05 \rho_{\text{Ref}}$ from current seismic wave reconstructions. And for question 3, we will compare the results for ρ_{Ref} with the ones from Profile₇. In addition, we will show the curves for $\bar{\rho}$ to estimate how far earlier studies have been off the more realistic calculations.

We show in Fig. 3 the $\sin^2 2\theta_{13}$ sensitivity as function of baseline. In the left panel, one can clearly see a minimum at about 7 300 km for Profile₇ from a single baseline optimization. The reference density ρ_{Ref} simulates the profile in an excellent way. Misjudging the matter density, however, can affect the sensitivity quite severely, and a slightly shorter baseline of $L \simeq 7\,000$ km may be safest from this point of view.⁴ However, from Fig. 3, right panel, one can read off that while the optimum is still at $L_2 \simeq 7\,500$ km, a baseline $L_2 \simeq 7\,500_{-500}^{+1\,000}$ km does not affect the combined result from two baselines significantly. Additionally, the exact prediction for the matter density profile is irrelevant. The reason is that the very long baseline acts as a degeneracy resolver which can lift the intrinsic and mass hierarchy degeneracies far enough irrespective of the exact baseline choice. Note that placing all detector mass at $L_1 = 4\,000$ km is shown for comparison (horizontal lines), and one can clearly see the order of magnitude improvement coming from the second baseline. We have checked these results for the combination with $L_1 = 3\,000$ km, and also for a larger value of Δm_{31}^2 . In both cases, none of the results change qualitatively. In addition, we show the impact of

⁴For a shorter baseline $L \simeq 7\,000$ km, the loss in sensitivity is much smaller when misjudging the matter density (such as actually having a 5% higher density) than for a baseline fine-tuned to 7 300 km.

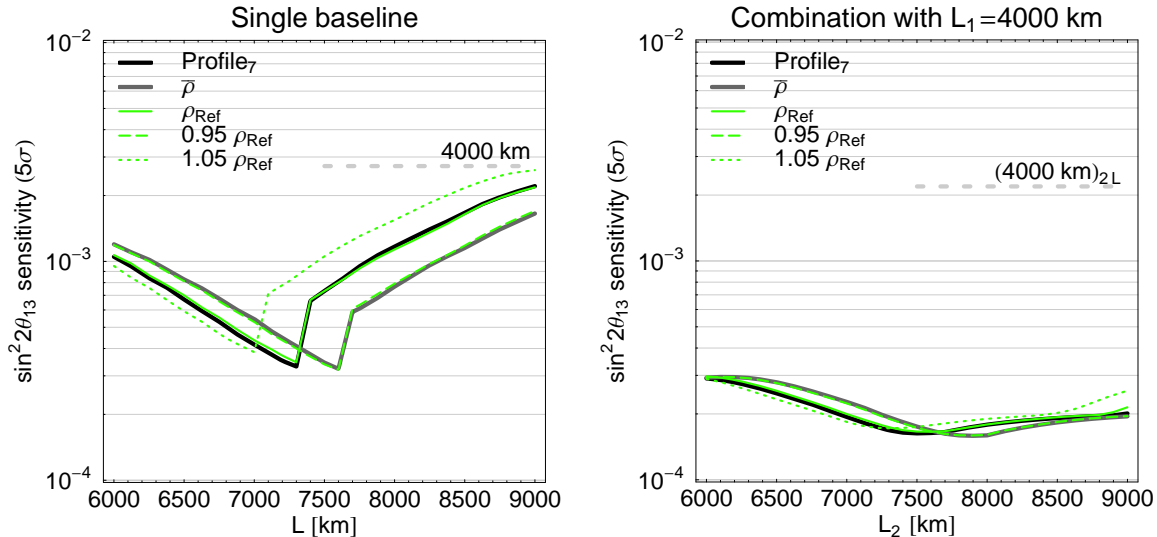


Figure 3: The $\sin^2 2\theta_{13}$ sensitivity as function of L including systematics, correlations, and degeneracies at the 5σ confidence level. The left plot corresponds to a single baseline only, while the right plot shows the combination with a shorter baseline $L_1 = 4000$ km. In both cases, placing all detector mass at $L = 4000$ km is shown for comparison as horizontal lines (the index “2L” refers to “double luminosity” because the detector mass in the right plot is twice as high as in the left plot). The different curves represent our different matter density models as represented in the plot legends.

a smaller detector mass at L_2 in Appendix A. We conclude that for the $\sin^2 2\theta_{13}$ sensitivity, the detector location can be chosen quite freely if there is sufficient statistics from a shorter baseline.⁵

Assuming the $\sin^2 2\theta_{13}$ sensitivity as our primary criterion for optimization, one can cross-check the results with the mass hierarchy and CP violation sensitivity. Note that an approach that assumes mass hierarchy and CP violation as primary optimization criteria would be much more complicated because one can optimize for two different degrees of freedom: $\sin^2 2\theta_{13}$ reach and δ_{CP} values (“Fraction of δ_{CP} ” for which one can discover the mass hierarchy or CP violation). In this study, we choose to use the fraction of δ_{CP} for different physics scenarios in $\sin^2 2\theta_{13}$ to cross-check the optimization. However, unless $\sin^2 2\theta_{13} \gtrsim 0.01$, it will not be possible to predict which scenario is actually realized in nature before a neutrino factory is built. Therefore, these physics scenarios can really only serve as cross-checks to predict how well the final setup would perform for certain hypothetical choices of simulated values.

It has been demonstrated in Ref. [23] that a very long baseline is absolutely necessary for the mass hierarchy determination if $\sin^2 2\theta_{13}$ is small. We have therefore checked the mass hierarchy sensitivity with this in mind and have found that hierarchy determination

⁵This has implications for the proposed INO detector [48], the location of which will be at distances of 6560 km from JHF and 7145 km from CERN, thus making it a suitable very long baseline detector.

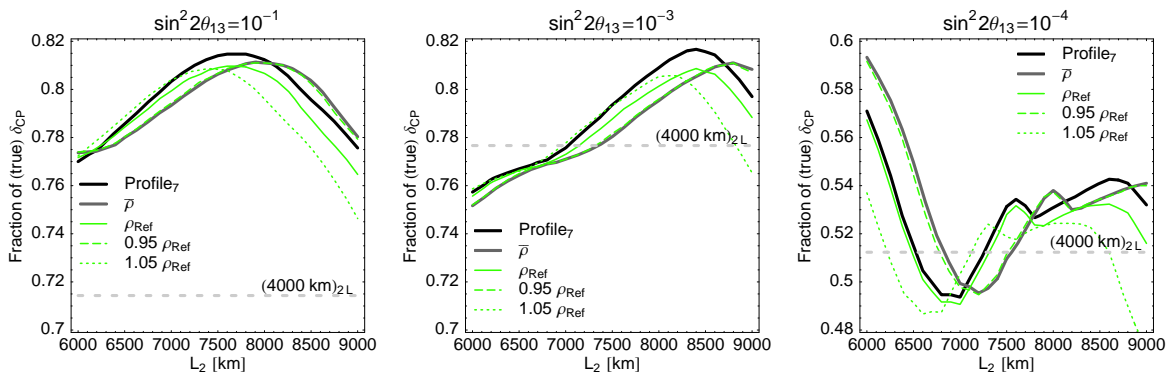


Figure 4: The “fraction of (true) δ_{CP} ” for which CP violation can be detected as function of L at the 3σ confidence level. This number represents the fraction of all possible values of δ_{CP} for which the CP conserving values $\delta_{\text{CP}} = 0$ and π can be excluded. The different panels correspond to different simulated values of $\sin^2 2\theta_{13}$, as given in the captions. In all cases, the results are shown in combination with a second baseline $L_1 = 4000$ km, and the reference curves for placing all detector mass at L_1 are shown as horizontal lines. The different curves represent our different matter density models as represented in the plot legends. For this figure, a normal mass hierarchy has been assumed.

should be easily possible for $L_1 = 4000$ km combined with L_2 in the window between 6000 and 9000 km for any value of δ_{CP} and $\sin^2 2\theta_{13} \gtrsim 10^{-4}$ at the 3σ confidence level (for any of the tested density models). Only at $\sin^2 2\theta_{13} \sim 10^{-4}$ does the baseline window $L_2 = (7300 \pm 200)$ km represent a local optimum (Fraction of $\delta_{\text{CP}} = 100\%$), but the loss in the fraction of δ_{CP} if one moves away from this optimal value is at most 20%.

It is well known that the short baseline plays a major role in enhancing the sensitivity to CP violation. Thus, in Fig. 4, we show the combination of $L_1 = 4000$ km and L_2 on the horizontal axes for the sensitivity to CP violation, where the long baseline serve primarily as a degeneracy resolver (note the scale on the vertical axes). For large and medium $\sin^2 2\theta_{13}$ (left and middle panels), one can read off that slightly longer baselines compared to the magic baseline are preferred. For example, for large $\sin^2 2\theta_{13}$, the optimum would be $L_2 = (7700 \pm 500)$ km. The reason for this pull to longer baselines is the δ_{CP} sensitivity returning for baselines longer than the magic baseline, *i.e.*, there is additional statistics on the CP violation measurement itself. This preference of longer baselines becomes more dominant for smaller values of $\sin^2 2\theta_{13}$, and is also accompanied by a narrowing of the peak. Only for very small values of $\sin^2 2\theta_{13}$ (right panel), does the magic baseline peak at ~ 7600 km become less pronounced because the measurement is statistics dominated and any baseline with some CP violation sensitivity helps. Again, placing all detector mass at 4000 km is shown for comparison by the horizontal lines. The increase of the physics performance by using the very long baseline is actually best for large $\sin^2 2\theta_{13}$, where the correlation with the matter effect affects the short baseline. Coming back to our main questions, Fig. 4 illustrates once more that ρ_{Ref} models the profile effect very well with respect to the positions of the peaks, while the peaks for $\bar{\rho}$ are slightly shifted. Note, however, that the absolute performance using the matter density profile is up to 1% better in the fraction

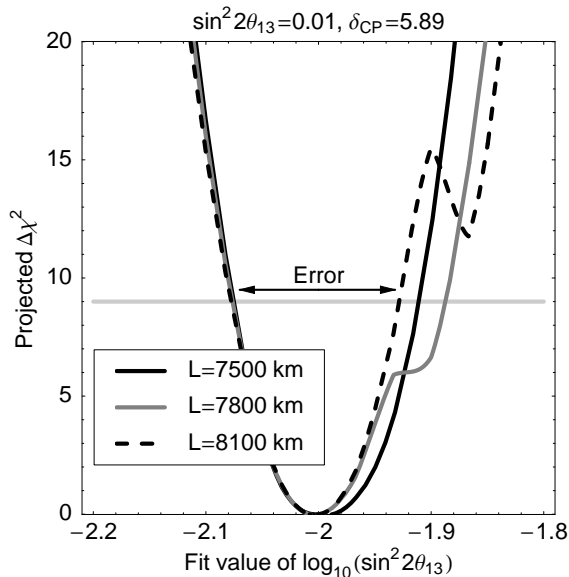


Figure 5: The (projected) $\Delta\chi^2$ as function of $\log_{10}(\sin^2 2\theta_{13})$ for the true values $\sin^2 2\theta_{13} = 0.01$ and $\delta_{\text{CP}} = 5.89$ for different baselines as given in the plot legend.

of δ_{CP} (profile effect). Misjudging the matter density is only relevant if it turns out to be much higher than anticipated and the chosen baseline is very long (effect up to several per cent). Taking into account all the information from this section, we conclude that the final choice of the very long baseline length may well be determined by the availability of detector locations and the storage ring design rather than from physics, because the combination of two baselines is rather insensitive to the very long baseline length and the specifics of the matter density profile. In particular, a baseline somewhat longer than the magic baseline does not downgrade the physics potential.

6 Application: $\sin^2 2\theta_{13}$ precision measurement

While it is obvious from the phenomenological point of view that a very long baseline is a robust correlation and degeneracy resolver, one could conceivably resolve these degenerate solutions by different approaches, such as increased statistics, an improved detector, or different oscillation channels. However, in this section, we will discuss an obvious generic application of a very long baseline: the precision of θ_{13} . In general, this measurement depends strongly on the true value of δ_{CP} [22]. Since, to leading order, there is no δ_{CP} -dependence at the magic baseline, it provides a low risk option for detector placement, in addition to the possibility of improved precision in θ_{13} .

We define the $\sin^2 2\theta_{13}$ precision as the full width relative error on $\log_{10}(\sin^2 2\theta_{13})$, *i.e.*,

$$\text{Rel. error on } \log_{10}(\sin^2 2\theta_{13}) \equiv \frac{\log_{10}(\sin^2 2\theta_{13})|_{\text{upper}} - \log_{10}(\sin^2 2\theta_{13})|_{\text{lower}}}{\log_{10}(\sin^2 2\theta_{13})|_{\text{true}}}, \quad (7)$$

where “upper” and “lower” refer to the most upper and lower intersections of the fitted $\Delta\chi^2$ with the line $\Delta\chi^2 = 9$. We do not include the $\text{sgn}(\Delta m_{31}^2)$ -degeneracy because it is hard to define the $\sin^2 2\theta_{13}$ precision including this information. The chosen value $\Delta\chi^2 = 9$ corresponds to the 3σ error for Gaussian errors, which is, strictly speaking, not always given in this case. We illustrate our definition in Fig. 5, where the (projected) $\Delta\chi^2$ is shown as function of $\log_{10}(\sin^2 2\theta_{13})$ for a specific set of true values. The error is obtained from the intersections with the horizontal line (see arrows). As one can easily see in this figure, the $(\delta_{\text{CP}}, \theta_{13})$ -degeneracy [20] is present in some cases under the chosen $\Delta\chi^2$. It is included in the error by our definition. One can also see from this figure that while at the magic baseline the $(\delta_{\text{CP}}, \theta_{13})$ -degeneracy is non-existent (no δ_{CP} -dependence), it reappears for longer baselines ($L = 7800$ km), but is quickly lifted over the chosen confidence level ($L = 8100$ km). Therefore, we expect jumps in the θ_{13} precision as a function of baseline wherever this lifting occurs.

We show in Fig. 6 the precision of $\sin^2 2\theta_{13}$ as function of the very long baseline length L . The left column corresponds to the very long baseline only, the right column to the combination with a shorter baseline at 4000 km. The different rows correspond to different (true) values of $\sin^2 2\theta_{13}$ as given in the plot captions. The dependence on the true value of δ_{CP} is shown by the bands: The upper ends correspond to the worst case δ_{CP} , the lower ends to the best case δ_{CP} , and the thick curves to the “typical value of δ_{CP} ”, *i.e.*, the median of the distribution (the precision will be better in 50% of all cases, and worse in the other 50%). The gray horizontal bands represent all detector mass at the short baseline.

Let us first of all focus on the left column of Fig. 6 and discuss the θ_{13} precision for a single very long baseline. There are two aspects which can be inferred from this figure: The absolute performance and the risk minimization with respect to δ_{CP} . For the absolute performance, compare, for instance, the thick dark curve for the “typical” δ_{CP} with the reference thick horizontal line for $L = 4000$ km. One can easily read off that in all cases of $\sin^2 2\theta_{13}$ (rows) a baseline of around 6700 km to 7700 km performs significantly better than the short baseline for the typical δ_{CP} . For large or small $\sin^2 2\theta_{13}$, this baseline window is even larger. As far as risk minimization is concerned, the worst case performance (upper ends of bands) is almost always better than for the short baseline, whereas the best case performance is only better for large $\sin^2 2\theta_{13}$. The reason is the importance of the matter density uncertainties for large $\sin^2 2\theta_{13}$ [41], which can be reduced by a clean determination of $\sin^2 2\theta_{13}$ at the very long baseline [23]. In addition, one can clearly see that the dependence on δ_{CP} is minimal at the magic baseline, where the bands become very narrow. The jumps in the best case precision come from the lifting of the $(\delta_{\text{CP}}, \theta_{13})$ -degeneracy as discussed above. In this case, the precision is determined by a different value of δ_{CP} , leading to the jump.

As for the combination of two baselines, we compare the very long baseline combined with 4000 km with all detector mass located at 4000 km (gray shaded region). In all cases, the best case, the worst case, and the median performance are better than for the short baseline only, which means that the combination of the two baselines is very synergistic. In particular, the performance for the typical δ_{CP} is much better for the combination than for one baseline only. In addition, there is much less sensitivity to the exact value of the very long baseline length compared to one baseline only. Note that the behavior as function of the

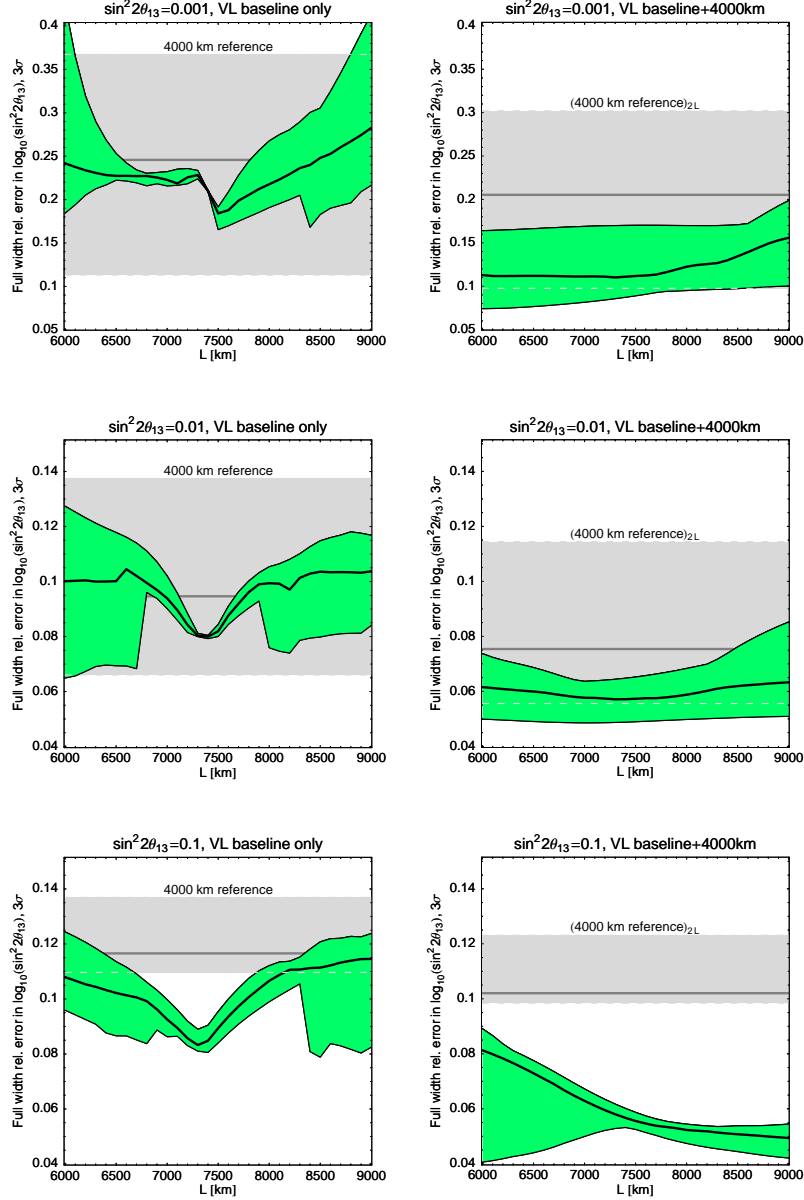


Figure 6: The precision of $\sin^2 2\theta_{13}$ (as defined in the main text) as function of the very long baseline length L . The left column corresponds to the very long baseline only, the right column to the combination with a shorter baseline at 4000 km. The different rows correspond to different (true) values of $\sin^2 2\theta_{13}$ as given in the plot captions. The dependence on the true value of δ_{CP} is shown by the bands: The upper ends correspond to the worst case δ_{CP} , the lower ends to the best case δ_{CP} , and the thick curves to the “typical value of δ_{CP} ”, *i.e.*, the median of the distribution (the precision will be better in 50% of all cases, and worse in the other 50%). The gray horizontal bands represent the short baseline only for reference (worst case, median, and best case). Note that in the right column, double luminosity was used for the reference (corresponding to all detector mass at 4000 km). In this figure, the reference density ρ_{Ref} was taken to simulate the matter density profile.

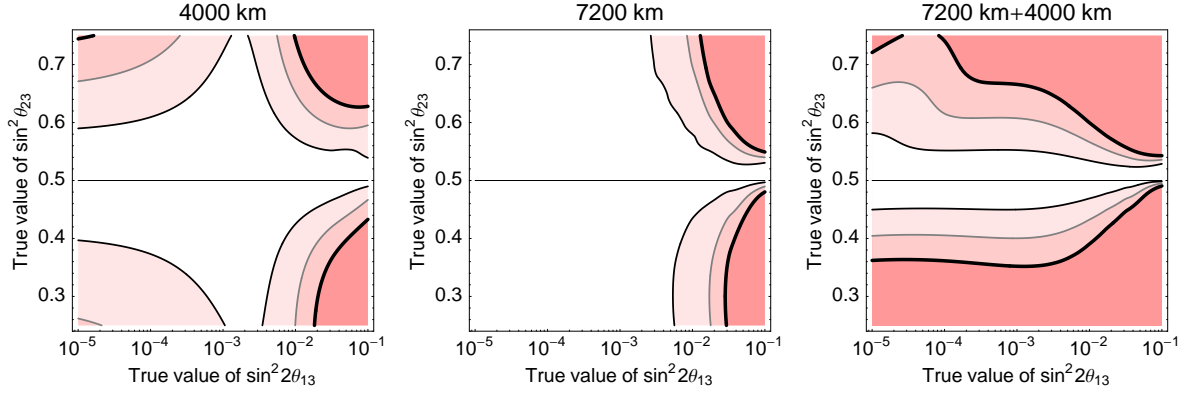


Figure 7: Regions where the $(\theta_{23}, \pi/2 - \theta_{23})$ -degeneracy can be resolved as function of $\sin^2 2\theta_{13}$ and $\sin^2 \theta_{23}$ for different baseline options as given in the plot labels. The different shadings represent the 1σ , 2σ , and 3σ confidence level sensitive regions (from light to dark, 1 d.o.f.). The different panels represent different baseline configurations. Here the true $\delta_{\text{CP}} = 0$ and a normal mass hierarchy is assumed. Note that this figure does not take into account the mixed degeneracy in $\text{sgn}(\Delta m_{31}^2)$ and $(\theta_{23}, \pi/2 - \theta_{23})$ combined.

baseline depends very much on $\sin^2 2\theta_{13}$: For small $\sin^2 2\theta_{13}$, shorter baselines are preferred because of better statistics, whereas for large $\sin^2 2\theta_{13}$, longer baselines are preferred since matter effects are dominant.⁶

7 Application: Resolving the $(\theta_{23}, \pi/2 - \theta_{23})$ -degeneracy

Another interesting application of a very long neutrino factory baseline is the resolution of the $(\theta_{23}, \pi/2 - \theta_{23})$ -degeneracy [43]. For example, at the magic baseline, we have from Eq. (1)

$$P_{e\mu}^{\text{Magic}} \simeq \sin^2 2\theta_{13} \sin^2 \theta_{23} \frac{\sin^2[(1 - \hat{A})\Delta]}{(1 - \hat{A})^2}, \quad (8)$$

which should be very sensitive to $\sin^2 \theta_{23}$ and therefore the octant at least for large $\sin^2 2\theta_{13}$. However, for small $\sin^2 2\theta_{13}$, $P_{e\mu}^{\text{Magic}} \simeq 0$ at this baseline, which means that there is no octant sensitivity. However, in the limit $\sin^2 2\theta_{13} \rightarrow 0$

$$P_{e\mu}^{\text{L}=4000 \text{ km}} \simeq \alpha^2 \cos^2 \theta_{23} \sin^2 2\theta_{12} \frac{\sin^2(\hat{A}\Delta)}{\hat{A}^2} \quad (9)$$

at the short baseline, which means that the octant degeneracy can, in principle, be resolved by the $\cos^2 \theta_{23}$ -dependence in the solar term at the shorter baseline. Note that this term

⁶The reason for the preference of longer baselines may actually be non-trivial: At the magic baseline, the $\sin(\hat{A}\Delta)$ -term in Eq. (1) changes sign. Therefore, for longer baselines, the role of δ_{CP} and $-\delta_{\text{CP}}$ is exchanged, *i.e.*, the risk with respect to δ_{CP} is lowered by the combination of the short and long baseline. Note that a similar behavior can be found for the silver channel at the short baseline: For maximal mixing, the probability is the same as for the golden channel except from $\delta_{\text{CP}} \rightarrow -\delta_{\text{CP}}$.

is suppressed by $\alpha^2 \sim 10^{-3}$, which means that the octant resolution will be considerably worse than for large $\sin^2 2\theta_{13}$. For intermediate $\sin^2 2\theta_{13}$, all terms in Eq. (1) will be present, which means that the sensitivity to the $(\theta_{23}, \pi/2 - \theta_{23})$ -degeneracy will be highly affected by correlations with δ_{CP} . We therefore expect that the very long baseline could help to resolve these correlations.

We define that the $(\theta_{23}, \pi/2 - \theta_{23})$ -degeneracy can be considered to have been eliminated if, for a given simulated θ_{23} , no degenerate solution with θ_{23} in the wrong octant (and the same mass hierarchy) fits the original solution at the chosen confidence level. In order to find the degeneracy, we marginalize over all oscillation parameters in the wrong octant. We show in Fig. 7 the sensitivity to exclusion of the $(\theta_{23}, \pi/2 - \theta_{23})$ -degeneracy as a function of $\sin^2 2\theta_{13}$ and $\sin^2 \theta_{23}$ for different baseline options. Obviously, for large $\sin^2 2\theta_{13}$, the very long baseline has the better sensitivity because it is less affected by correlations with δ_{CP} . For small $\sin^2 2\theta_{13}$, the short baseline can still resolve the degeneracy, but with a very poor reach in $\sin^2 \theta_{23}$. For medium $\sin^2 2\theta_{13}$, there is no sensitivity for either baseline because the short baseline is affected by correlations, and the long baseline has intrinsically no sensitivity. However, the combination of the two baselines does very well in a wide range of $\sin^2 2\theta_{13}$ because the long baseline helps to constrain $\sin^2 2\theta_{13}$ very well. Note that we do not show the sensitivity to the mixed (octant and sign) degeneracy in this analysis, which would impose the additional requirement that the mass hierarchy be resolved (*cf.*, *e.g.*, Ref. [49]). In addition, our results are quantitatively comparable with the ones in Ref. [31] for the individual baselines. As far as the dependence on δ_{CP} is concerned, we do not expect a qualitatively interesting behavior, see Refs. [31, 49].

It is possible that an octant degeneracy resolution may be obtained earlier than from a neutrino factory by atmospheric plus long-baseline data [49, 50], reactor plus long-baseline data [9, 51, 52], or long-baseline plus astrophysical data [53, 54].⁷ For large $\sin^2 2\theta_{13}$, a neutrino factory would be very competitive to all of these these methods. For small $\sin^2 2\theta_{13}$, a determination from atmospheric (or possibly astrophysical) data combined with long-baseline data could come earlier. However, it would require a megaton-size water Cherenkov detector and megawatt-class superbeam upgrade. From a practical point of view, it appears likely that only one of these combinations (neutrino factory or superbeam upgrade) will be eventually realized.

Finally, we have examined, as a different approach, the efficiency of the silver channel at the magic baseline as a degeneracy resolver. At this baseline, we have (see, *e.g.*, Ref. [29])

$$P_{e\tau}^{\text{Magic}} \simeq \sin^2 2\theta_{13} \cos^2 \theta_{23} \frac{\sin^2[(1 - \hat{A})\Delta]}{(1 - \hat{A})^2}. \quad (10)$$

Therefore, using Eq. (8), the ratio $P_{e\mu}/P_{e\tau} = \tan^2 \theta_{23}$ should determine the octant degeneracy without being spoilt by any correlations and degeneracies. We have tested the silver channel for the implementation in Refs. [23, 56] with a 10 kt emulsion cloud chamber and 4 yr of ν_τ appearance, and we have not found a significant contribution to the two baseline combination. However, the silver channel does help somewhat for the very long baseline alone for intermediate $\sin^2 2\theta_{13}$. The reason for the marginal contribution is the very low

⁷See also Ref. [55] for atmospheric data alone and large θ_{13} .

True value of $\sin^2 2\theta_{13}$	Measurement of ρ_{Ref}			Measurement of ρ_{LM}		
	1σ	2σ	3σ	1σ	2σ	3σ
$\sin^2 2\theta_{13} = 0.1$	+0.0024 -0.0024	+0.0047 -0.0047	+0.0071 -0.0071	+0.0025 -0.0025	+0.0050 -0.0050	+0.0075 -0.0076
$\sin^2 2\theta_{13} = 0.01$	+0.0065 -0.0065	+0.013 -0.013	+0.020 -0.019	+0.0069 -0.0068	+0.014 -0.014	+0.021 -0.020
$\sin^2 2\theta_{13} = 0.001$	+0.021 -0.019	+0.043 -0.038	+0.067 -0.056	+0.021 -0.020	+0.043 -0.040	+0.068 -0.059

Table 1: Relative precision of the measurement of ρ_{Ref} (constant density along baseline) and ρ_{LM} (lower mantle part of the baseline only) at different confidence levels and for different values of $\sin^2 2\theta_{13}$. The same parameters as in Fig. 8 are used. Note that for the ρ_{LM} precision in this table, the upper mantle density is assumed to be known/fixed. This constraint is studied in Fig. 9.

event rate in the silver channel at this baseline, *i.e.*, low statistics (about 176 signal events for $\sin^2 2\theta_{13} = 0.1$).

8 Application: Matter density measurement

As mentioned earlier, the sensitivity to matter density changes at the magic baseline is high. Moreover, the fact that matter density uncertainties affect the extraction of $\sin^2 2\theta_{13}$ and δ_{CP} for large $\sin^2 2\theta_{13}$ is well known (see, *e.g.*, Ref. [41]). This implies that one can extract some information on the matter density as well. Such neutrino oscillation tomography using a neutrino beam has, for example, been studied in Refs. [57–60]. In this section, we discuss the use of neutrino data for potential geophysics applications as a by-product of a very long neutrino factory baseline. We stress however that the primary purpose of such a baseline remains its use as a degeneracy resolver for neutrino oscillation physics, and the geophysics would be a nice addition coming for free. However, if there are different alternative detector locations, the geophysics along the neutrino factory baseline might have some impact on the choice of the location.

We follow the treatment of the matter density measurement in Ref. [59] described in Sec. 3, *i.e.*, we use the information from both the short ($L = 4000$ km) and the very long baseline to reduce the impact of correlations. For the short baseline, we use the mean density in Eq. (4) and allow for a 5% matter density uncertainty. For the long baseline, we will use several models for the density measurement as described below. Note that all of the oscillation parameters are marginalized over, *i.e.*, their uncertainties are taken into account.

As a first model, let us assume that we measure the constant density along the baseline modeled by ρ_{Ref} (*cf.*, Sec. 4). The precision of this measurement is shown in Fig. 8 as function of $\sin^2 2\theta_{13}$ (and in Table 1 for specific values of $\sin^2 2\theta_{13}$). For large $\sin^2 2\theta_{13}$, where the δ_{CP} -terms in Eq. (1) are small relative to the first term, the measurement is very precise and dominated by a combination of resonance peak position and probability suppression at high energies, *i.e.*, the characteristic spectral dependence of the matter effect (*cf.*, Ref. [60]). For small $\sin^2 2\theta_{13}$, however, the measurement is dominated by the α^2 -term in Eq. (1), which does not have the resonance information and therefore has a lower precision. For medium $\sin^2 2\theta_{13}$, the δ_{CP} -terms act as a background to the density extraction, which

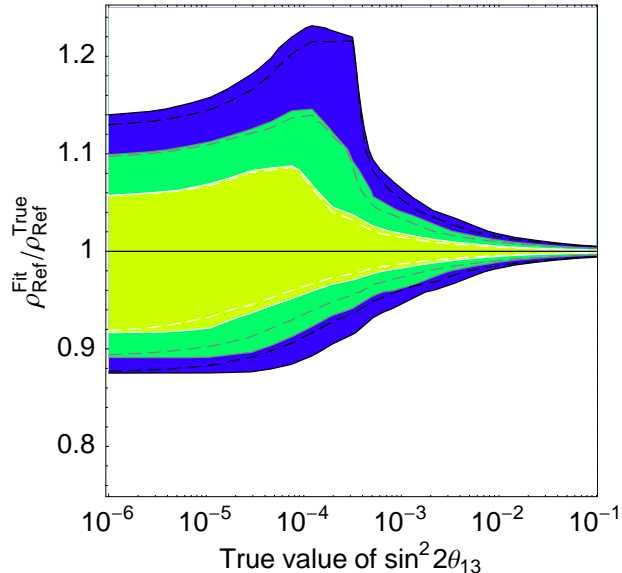


Figure 8: Relative precision of the density measurement of ρ_{Ref} as function of $\sin^2 2\theta_{13}$ at the 1σ , 2σ , and 3σ confidence levels (contours from light to dark). For the baseline, we have chosen $L = 7500$ km in combination with $L = 4000$ km used to measure the oscillation parameters, as well as we have assumed a normal mass hierarchy and $\delta_{\text{CP}} = 0$. The dashed curves correspond to not taking into account the correlations with the oscillation parameters, which means that the shown combination is close to optimal.

means that the signal is least clean and the performance is worst there. Note that at the magic baseline only the $\sin^2 2\theta_{13}$ -term is present by definition. However, the suppression of the other terms by $\sin(\hat{A}\Delta) = 0$ depends on our knowledge of the matter density, which means that any deviations in the matter density make these terms return.

As an alternative model, one can also think about measuring the density along the baseline part in a depth $d \gtrsim 670$ km penetrating the lower mantle of the Earth (*cf.*, Fig. 1, left, where the inner density jumps occur). We call this density the lower mantle mean density ρ_{LM} along our baseline, which corresponds to the top density in Profile₇. If we assume that we know the upper mantle density profile exactly, we obtain the precisions in Table 1, where we also compare them to the measurement of ρ_{Ref} . For large $\sin^2 2\theta_{13}$, we find that one can measure the density up to 0.25% at 1σ or 0.75% at 3σ . These precisions are very competitive to geophysics and could be used to discriminate among different seismic models.

For a slightly more realistic modeling of the ρ_{LM} measurement, the obtainable precision will certainly depend on the local knowledge of the upper mantle (and crust) density close to source and detector. This is illustrated by the depth curve in Fig. 1, left, which relatively quickly goes into the lower mantle section. Assuming that Eq. (4) describes the density measurement to first order, we suspect that the upper and lower mantle densities are highly correlated, *i.e.*, for instance, a lower density in the upper mantle can partly be compensated by a higher density in the lower mantle. Therefore, we perform a combined fit and discuss the precision of ρ_{LM} as function of the error in the upper mantle (and crust) density. Note

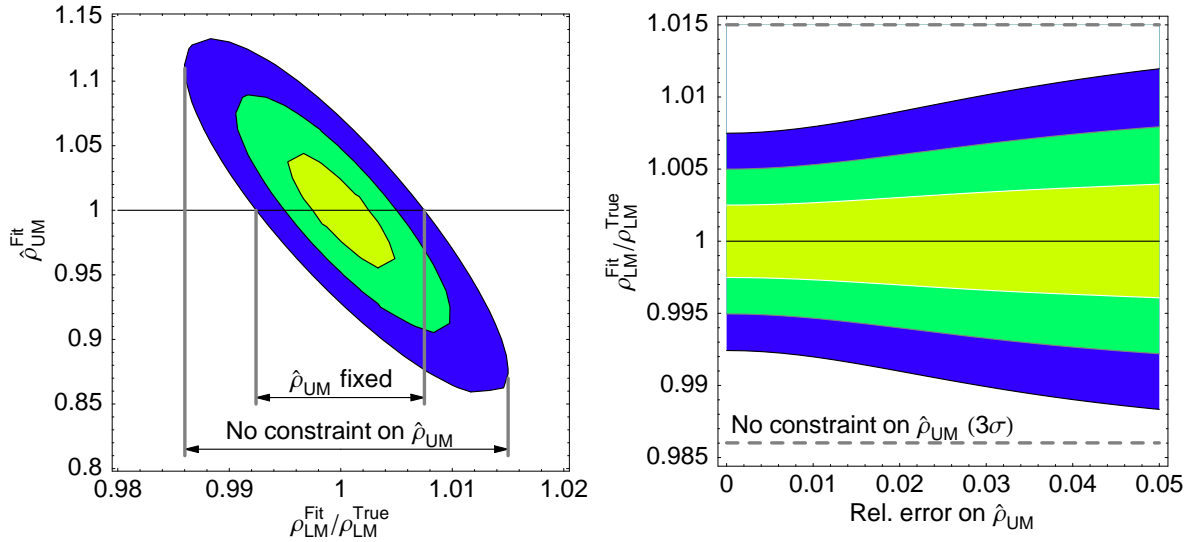


Figure 9: Left plot: Correlation between lower mantle density ρ_{LM} and normalization of the upper mantle/crust density $\hat{\rho}_{UM}$. The arrows indicate the error on ρ_{LM} for no constraint on $\hat{\rho}_{UM}$ and a very precise knowledge on $\hat{\rho}_{UM}$. Right plot: Precision of ρ_{LM} as function of relative external error on $\hat{\rho}_{UM}$. The dashed lines refer to the no constraint limit. Both plots show the 1σ , 2σ , and 3σ errors (from light to dark, 1 d.o.f.) for $\sin^2 2\theta_{13} = 0.1$. Here we have chosen $L = 7500$ km.

that we only use two parameters in this model: The density ρ_{LM} , which we want to measure, and an overall density normalization $\hat{\rho}_{UM}$ for the profile in the upper mantle, which we will marginalize over.

The result of this analysis can be found in Fig. 9. In the left plot, the correlation between ρ_{LM} and $\hat{\rho}_{UM}$ is shown. Because the baseline only runs a short distance in the upper mantle, the upper mantle density normalization needs to deviate substantially from unity to cause a major effect in ρ_{LM} (*cf.*, scales on axes). The arrows indicate the error on ρ_{LM} for no constraint on $\hat{\rho}_{UM}$ and a very precise knowledge on $\hat{\rho}_{UM}$. In the right plot of Fig. 9, we impose an external (Gaussian) 1σ -error on $\hat{\rho}_{UM}$ which represents the precision we believe in the upper mantle density close to the chosen source and detector locations. We show the precision of ρ_{LM} as function of this relative external error on $\hat{\rho}_{UM}$. As one can easily read off this figure, the impact of the upper mantle-lower mantle density correlation will be very small as long as one knows the upper mantle density at the chosen location better than about 2%, and even for 5%, representing the worst case, the deviation from the best case is not very strong.

We have also tested the dependence of the measurement on the baseline and we have not found a significant change in the precision as long as $L \gtrsim 7000$ km. However, not surprisingly, there is a slight optimum at the magic baseline for medium $\sin^2 2\theta_{13}$, because the δ_{CP} -dependence is suppressed there. In addition, we have tested the improved neutrino factory from Ref. [23] and have found a considerably higher precision if the muon

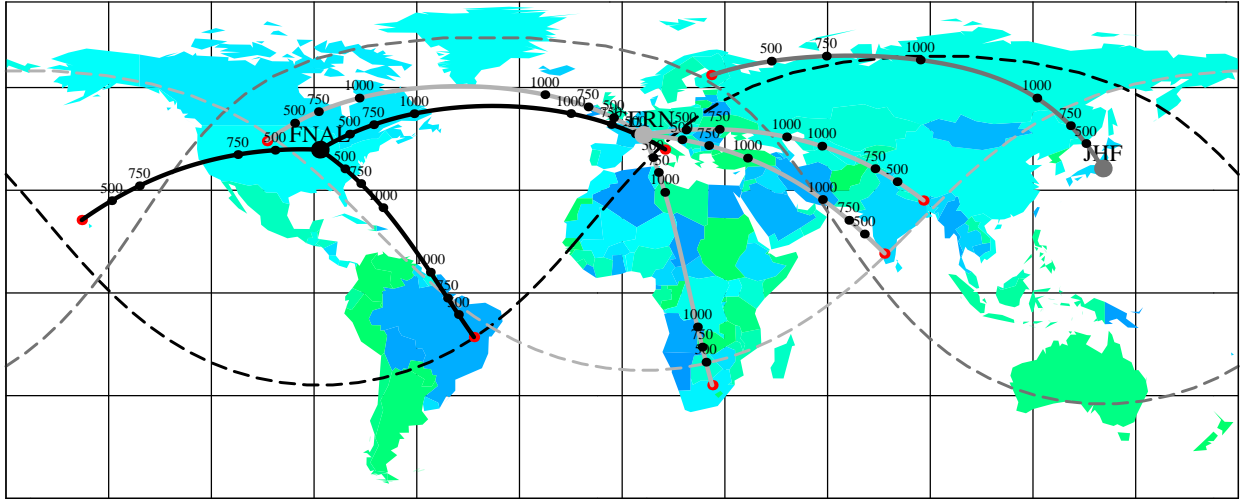


Figure 10: Different major potential neutrino factory host laboratories, all corresponding detector locations at $L = 7200$ km (dashed curves, corresponding colors), and several chosen baselines to specific potential detector locations (red points/end points of curves) projected onto the Earth's surface (solid curves). Along these baselines the depth is given in kilometers at several selected points.

energy is not lowered to 20 GeV. The reason is that the precision part comes from the high energy part of the spectrum. Furthermore, we do not expect a quantitatively very different result for different values of δ_{CP} or the mass hierarchy in the high precision limit, because the δ_{CP} -dependence is of secondary importance for large $\sin^2 2\theta_{13}$, and we have considered symmetric operation of the neutrino factory symmetric with respect to neutrinos and antineutrinos. For details of the parameter dependencies, see also Ref. [60]. Note that compared to Ref. [60], we find slightly higher precisions for large $\sin^2 2\theta_{13}$, because we use the full spectral information (in 43 energy bins) and the knowledge from the short baseline.

As far as the geophysical interpretation and the selection of detector locations are concerned, we show in Fig. 10 different major potential neutrino factory host laboratories and several chosen baselines to specific potential detector locations (red points/end points of curves) projected onto the Earth's surface (solid curves). Along these baselines the depth is given in kilometers at several selected points. Comparing Fig. 10 with seismic wave reconstructions (see, *e.g.*, Ref. [61]), one can read off that the obtainable precision on ρ_{LM} is sufficient for a 3σ discrimination of different seismic wave reconstructions at specific places, and possibly sufficient for the discrimination of different geophysical hypotheses. However, we leave the drawing of stronger conclusions based on these results to experts in geophysics.

9 Physics case for a very long baseline $6\,000\text{ km} \lesssim L \lesssim 9\,000\text{ km}$

In this section, we summarize the results from this and earlier studies to qualitatively review the physics case for a very long neutrino factory baseline. We demonstrate that such a baseline is extremely versatile over the full allowed range of values of $\sin^2 2\theta_{13}$, even if the specific advantages it has differ for low, medium and high values of this parameter. Note

that we focus on the baseline window $6\,000\text{ km} \lesssim L \lesssim 9\,000\text{ km}$ used for this study.

All allowed values of $\sin^2 2\theta_{13}$

A very long baseline helps for the precision measurements of Δm_{31}^2 and especially θ_{23} , where, as a general rule of thumb, the longer the baseline, the better [23]. Furthermore, as illustrated in Sec. 7, the ability of a shorter baseline to resolve the $(\theta_{23}, \pi/2 - \theta_{23})$ -degeneracy is significantly improved for all values of $\sin^2 2\theta_{13}$. In addition, the very long baseline improves the $\sin^2 2\theta_{13}$ precision measurement in all practical cases when $\sin^2 2\theta_{13}$ is large enough such that this measurement is relevant. It also minimizes the uncertainty stemming from the unknown value of δ_{CP} (*cf.*, Sec. 6).

Large $\sin^2 2\theta_{13} \gtrsim 10^{-2}$

For large $\sin^2 2\theta_{13}$, the very long baseline helps to reduce the impact of the matter density uncertainties by increasing the accuracy in the measurement of $\sin^2 2\theta_{13}$, which means that the CP violation potential of the short baseline becomes significantly enhanced [23]. Note that in this case, an improved knowledge of the matter density profile becomes unimportant. Therefore, the very long baseline could be one of the key elements in establishing the physics case for a neutrino factory for large $\sin^2 2\theta_{13}$. In fact, the very long baseline can even measure the matter density along its length to an extremely high precision competitive with geophysical techniques, which may provide additional information on the Earth's lower mantle (*cf.*, Sec. 8 and Ref. [60]).

Medium $10^{-3} \lesssim \sin^2 2\theta_{13} \lesssim 10^{-2}$

In this scenario, the very long baseline guarantees the mass hierarchy sensitivity for all values of δ_{CP} , and it resolves correlation and degeneracies affecting the CP violation performance [23]. In addition, the δ_{CP} precision measurement, which strongly depends on the true value of δ_{CP} itself for the short baseline only, becomes a low risk endeavor [62]. Furthermore, there may still be valuable constraints on the matter density profile (*cf.*, Sec. 8 and Ref. [60]).

Small $10^{-4} \lesssim \sin^2 2\theta_{13} \lesssim 10^{-3}$

In this case, the main usefulness of the very long baseline lies in improving the $\sin^2 2\theta_{13}$ and mass hierarchy sensitivities [23,25]. In particular, the mass hierarchy discovery is guaranteed for all values of δ_{CP} , and the CP violation discovery will be possible for at least 50% of all values of δ_{CP} [23].

“Zero” $\sin^2 2\theta_{13} (\ll 10^{-4})$

Even if $\sin^2 2\theta_{13}$ is far below the limit of a neutrino factory and δ_{CP} becomes unmeasurable, there are several interesting measurements which can only be done with a very long baseline. For example, the MSW effect in Earth matter could still be verified at a very high confidence level because the solar appearance term is large enough [63]. This term would also allow for some information on the octant (see above). In addition, the disappearance data could be used towards a possible future measurement of the neutrino mass hierarchy [64]. Finally, this case may be very interesting from the theoretical point of view since it points towards either an exact or softly broken symmetry.

10 Summary and conclusions

We have studied the physics and applications of a very long neutrino factory baseline. Our work was primarily motivated by the magic baseline ($L \sim 7\,500$ km) where correlations and degeneracies naturally disappear. One of the important questions has been the modeling of the matter density profile, because the density is crucial for the determination of the magic baseline length. We have found that the optimal constant density describing the physics at such a baseline is about 5% higher than the average matter density at this baseline. Note that this optimal density also describes profile effects with sufficient accuracy. This implies that the magic baseline is significantly shorter than one may naively infer, a conclusion that has significant implications for decisions on future detector locations.

Furthermore, we have re-investigated the baseline optimization for different matter profile assumptions. While a single baseline optimization (magic baseline only) is very sensitive to errors in the assumed density profile, we have demonstrated that the combination with a shorter baseline $L \simeq 4\,000$ km allows for a much larger baseline window for detector placement. In particular, for CP violation measurements, much longer baselines $L \sim 7\,500$ to $8\,500$ km could even be preferable, or, at least, do not harm.

As far as potential applications of a very long baseline are concerned, the primary purpose remains degeneracy resolution. Beyond that, we have demonstrated other interesting applications. For example, we have shown that such a baseline allows for a low risk (with respect to δ_{CP}) $\sin^2 2\theta_{13}$ precision measurement, which is, in the worst case, as well as on the average, significantly better than for a short baseline only. In addition, we have illustrated the importance of the very long baseline for the octant degeneracy resolution for intermediate $10^{-4} \lesssim \sin^2 2\theta_{13} \lesssim 10^{-2}$. Finally, we have demonstrated that one can also extract the matter density along the baseline with a precision of about 0.24% (1σ). If one only wants to extract the average lower mantle density of the Earth along the baseline, we still find a precision of about 0.4% for a 5% matter density uncertainty in the upper mantle (and crust).

The physics case for a very long neutrino factory baseline has been summarized in Sec. 9. Depending on $\sin^2 2\theta_{13}$, this baseline has different applications and advantages, but it implies rich possibilities for all scenarios. Therefore, we conclude that a very long neutrino factory baseline would be an extremely versatile tool for a broad spectrum of physics scenarios, and

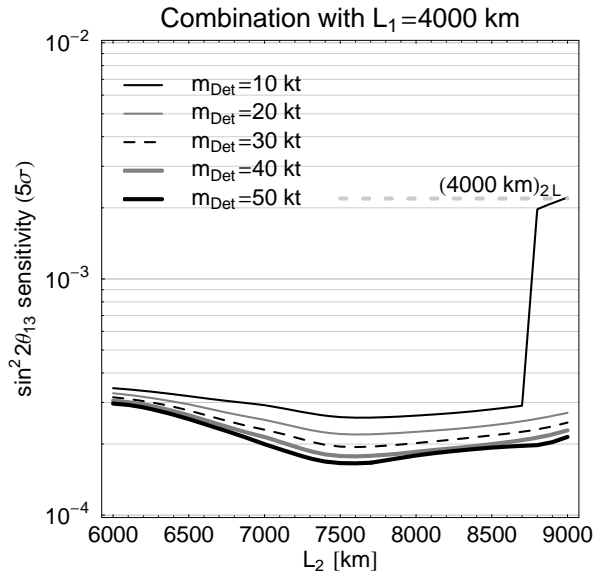


Figure 11: Same as Fig. 3, right, for different detector masses at the very long baseline L_2 as given in the plot legend (the detector mass at $L_1 = 4000$ km is fixed to 50 kt). For the matter density profile, the reference density ρ_{Ref} is used.

strongly warrants inclusion in the planning of a future neutrino factory complex.

Acknowledgments

We would like to thank Evgeny Akhmedov, Hisakazu Minakata, and the conveners and contributors of the ISS study for useful discussions. In addition, WW would like to acknowledge support from the W. M. Keck Foundation through a grant-in-aid to the Institute for Advanced Study, and through NSF grant PHY-0503584 to the Institute for Advanced Study, where parts of this work have been carried out, as well as funding by the Emmy Noether program of Deutsche Forschungsgemeinschaft. RG also thanks the Institute for Advanced Study, Princeton, for hospitality.

A How much detector mass is needed at the very long baseline?

In order to test the impact of detector mass, we show as one example in Fig. 11 the dependence of the $\sin^2 2\theta_{13}$ sensitivity on the very long baseline detector mass for the combination with the shorter baseline. One can easily see that $m_{\text{Det}} \gtrsim 20$ kt at the very long baseline is a safe choice, because smaller detector masses lead to a too large loss of events for baselines $L_2 \gtrsim 8500$ km.

References

- [1] J. Ellis (2006), [hep-ph/0611237](#).
- [2] T. Schwetz, *Phys. Scripta* **T127**, 1 (2006), [hep-ph/0606060](#).
- [3] S. Goswami, *Int. J. Mod. Phys.* **A21**, 1901 (2006).
- [4] G. L. Fogli, E. Lisi, A. Marrone, A. Palazzo, and A. M. Rotunno, *Prog. Part. Nucl. Phys.* **57**, 71 (2006).
- [5] M. Maltoni, T. Schwetz, M. A. Tortola, and J. W. F. Valle, *New J. Phys.* **6**, 122 (2004), [hep-ph/0405172](#).
- [6] E. Ables *et al.* (MINOS) FERMILAB-PROPOSAL-P-875.
- [7] Y. Itow *et al.* (2001), [hep-ex/0106019](#).
- [8] D. S. Ayres *et al.* (NOvA) (2004), [hep-ex/0503053](#).
- [9] H. Minakata, H. Sugiyama, O. Yasuda, K. Inoue, and F. Suekane, *Phys. Rev.* **D68**, 033017 (2003), [hep-ph/0211111](#).
- [10] P. Huber, M. Lindner, T. Schwetz, and W. Winter, *Nucl. Phys.* **B665**, 487 (2003), [hep-ph/0303232](#).
- [11] K. Anderson *et al.* (2004), [hep-ex/0402041](#).
- [12] F. Ardellier *et al.* (2004), [hep-ex/0405032](#).
- [13] S. Geer, *Phys. Rev.* **D57**, 6989 (1998), [hep-ph/9712290](#).
- [14] C. Albright *et al.* (2000), [hep-ex/0008064](#), and references therein.
- [15] M. Apollonio *et al.* (2002), [hep-ph/0210192](#).
- [16] V. D. Barger, S. Geer, R. Raja, and K. Whisnant, *Phys. Rev.* **D62**, 013004 (2000), [hep-ph/9911524](#).
- [17] V. Barger, S. Geer, and K. Whisnant, *Phys. Rev.* **D61**, 053004 (2000), [hep-ph/9906487](#).
- [18] V. D. Barger, S. Geer, R. Raja, and K. Whisnant, *Phys. Lett.* **B485**, 379 (2000), [hep-ph/0004208](#).
- [19] A. Cervera *et al.*, *Nucl. Phys.* **B579**, 17 (2000), [hep-ph/0002108](#).
- [20] J. Burguet-Castell, M. B. Gavela, J. J. Gomez-Cadenas, P. Hernandez, and O. Mena, *Nucl. Phys.* **B608**, 301 (2001), [hep-ph/0103258](#).
- [21] J. Burguet-Castell, M. B. Gavela, J. J. Gomez-Cadenas, P. Hernandez, and O. Mena, *Nucl. Phys.* **B646**, 301 (2002), [hep-ph/0207080](#).

- [22] P. Huber, M. Lindner, and W. Winter, Nucl. Phys. **B645**, 3 (2002), [hep-ph/0204352](#).
- [23] P. Huber, M. Lindner, M. Rolinec, and W. Winter, Phys. Rev. **D74**, 073003 (2006), [hep-ph/0606119](#).
- [24] V. Barger, D. Marfatia, and K. Whisnant, Phys. Rev. **D65**, 073023 (2002), [hep-ph/0112119](#).
- [25] P. Huber and W. Winter, Phys. Rev. **D68**, 037301 (2003), [hep-ph/0301257](#).
- [26] ISS detector working group, private communication.
- [27] R. Gandhi, P. Ghoshal, S. Goswami, P. Mehta, and S. Uma Sankar, Phys. Rev. **D73**, 053001 (2006), [hep-ph/0411252](#).
- [28] R. Gandhi, P. Ghoshal, S. Goswami, P. Mehta, and S. Uma Sankar, Phys. Rev. Lett. **94**, 051801 (2005), [hep-ph/0408361](#).
- [29] E. K. Akhmedov, R. Johansson, M. Lindner, T. Ohlsson, and T. Schwetz, JHEP **04**, 078 (2004), [hep-ph/0402175](#).
- [30] S. K. Agarwalla, A. Raychaudhuri, and A. Samanta, Phys. Lett. **B629**, 33 (2005), [hep-ph/0505015](#).
- [31] A. Donini, E. Fernandez-Martinez, D. Meloni, and S. Rigolin, Nucl. Phys. **B743**, 41 (2006), [hep-ph/0512038](#).
- [32] S. K. Agarwalla, S. Choubey, and A. Raychaudhuri (2006), [hep-ph/0610333](#).
- [33] A. Y. Smirnov (2006), [hep-ph/0610198](#).
- [34] M. Freund, Phys. Rev. **D64**, 053003 (2001), [hep-ph/0103300](#).
- [35] L. Wolfenstein, Phys. Rev. **D17**, 2369 (1978).
- [36] P. Huber, M. Lindner, and W. Winter, Comput. Phys. Commun. **167**, 195 (2005), <http://www.mpi-hd.mpg.de/lin/globes>, [hep-ph/0407333](#).
- [37] G. L. Fogli, E. Lisi, A. Marrone, and D. Montanino, Phys. Rev. **D67**, 093006 (2003), [hep-ph/0303064](#).
- [38] J. N. Bahcall, M. C. Gonzalez-Garcia, and C. Pena-Garay, JHEP **08**, 016 (2004), [hep-ph/0406294](#).
- [39] A. Bandyopadhyay, S. Choubey, S. Goswami, S. T. Petcov, and D. P. Roy (2004), [hep-ph/0406328](#).
- [40] R. J. Geller and T. Hara, Nucl. Instrum. Meth. **A503**, 187 (2001), [hep-ph/0111342](#).
- [41] T. Ohlsson and W. Winter, Phys. Rev. **D68**, 073007 (2003), [hep-ph/0307178](#).
- [42] H. Minakata and H. Nunokawa, JHEP **10**, 001 (2001), [hep-ph/0108085](#).

- [43] G. L. Fogli and E. Lisi, Phys. Rev. **D54**, 3667 (1996), [hep-ph/9604415](#).
- [44] T. Ohlsson and H. Snellman, Eur. Phys. J. **C20**, 507 (2001), [hep-ph/0103252](#).
- [45] T. Ohlsson and H. Snellman, Phys. Lett. **B474**, 153 (2000), [hep-ph/9912295](#).
- [46] T. Ota and J. Sato, Phys. Rev. **D63**, 093004 (2001), [hep-ph/0011234](#).
- [47] E. K. Akhmedov, Phys. Lett. **B503**, 133 (2001), [hep-ph/0011136](#).
- [48] M. S. Athar *et al.* (INO) A Report of the INO Feasibility Study, available at <http://www.imsc.res.in/~ino/OpenReports/report.html>.
- [49] P. Huber, M. Maltoni, and T. Schwetz, Phys. Rev. **D71**, 053006 (2005), [hep-ph/0501037](#).
- [50] J. E. Campagne, M. Maltoni, M. Mezzetto, and T. Schwetz (2006), [hep-ph/0603172](#).
- [51] K. B. McConnel and M. H. Shaevitz (2004), [hep-ex/0409028](#).
- [52] K. Hiraide *et al.*, Phys. Rev. **D73**, 093008 (2006), [hep-ph/0601258](#).
- [53] P. D. Serpico, Phys. Rev. **D73**, 047301 (2006), [hep-ph/0511313](#).
- [54] W. Winter, Phys. Rev. **D74**, 033015 (2006), [hep-ph/0604191](#).
- [55] S. Choubey and P. Roy, Phys. Rev. **D73**, 013006 (2006), [hep-ph/0509197](#).
- [56] D. Autiero *et al.*, Eur. Phys. J. **C33**, 243 (2004), [hep-ph/0305185](#).
- [57] T. Ohlsson and W. Winter, Europhys. Lett. **60**, 34 (2002), [hep-ph/0111247](#).
- [58] T. Ohlsson and W. Winter, Phys. Lett. **B512**, 357 (2001), [hep-ph/0105293](#).
- [59] W. Winter, Phys. Rev. **D72**, 037302 (2005), [hep-ph/0502097](#).
- [60] H. Minakata and S. Uchinami (2006), [hep-ph/0612002](#).
- [61] S. V. Panasyuk, *REM (Reference Earth Model) web page* (2000), <http://cfauvcs5.harvard.edu/lana/rem/index.htm>.
- [62] P. Huber, M. Lindner, and W. Winter, JHEP **05**, 020 (2005), [hep-ph/0412199](#).
- [63] W. Winter, Phys. Lett. **B613**, 67 (2005), [hep-ph/0411309](#).
- [64] A. de Gouvea and W. Winter, Phys. Rev. **D73**, 033003 (2006), [hep-ph/0509359](#).